PROBING THE BROAD EMISSION LINE OF QUASARS USING GRAVITATIONAL MICROLENSING

The Different Origins of High- and Low-Ionization Broad Emission Lines Revealed by Gravitational Microlensing in the Einstein Cross

L. Braibant[1], D. Hutsemékers[1], D. Sluse[1], T. Anguita[2]

[1] Institut d'Astrophysique, Université de Liège, Allée du 6 Août 17, B5c, 4000 Liège, Belgium
[2] Departamento de Ciencias Fisicas, Universidad Andres Bello, Av. Republica 252, Santiago, Chile
[3] Millennium Institute of Astrophysics, Chile

Introduction

When a quasar is lensed into multiple distorted images by a foreground massive galaxy, the dense field of stars in that lensing galaxy produces, in the source plane, a magnification pattern constituted of narrow highly-magnifying caustics (Fig. 1) that can sample and magnify the spatial and velocity structure of the ionized gas flowing close by the supermassive black hole at the center of quasars and at the origin of the broad emission lines observed in their spectra. This results in line profile distortions that depend on the geometry and kinematics of that broad emission line region (BLR), on the one hand, and on the caustic pattern, on the other hand. Microlensing thus constitutes a powerful tool to study the unresolved BLR of quasars.

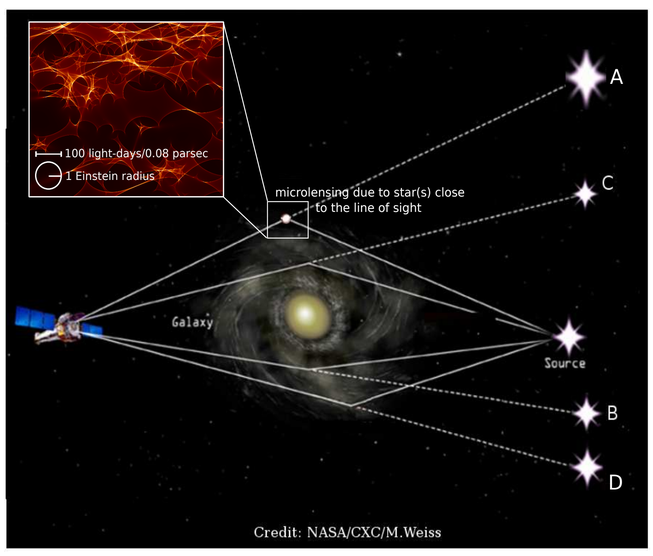

Fig. 1: *Gravitational lensing and microlensing. The icaustic network is computed for the image A of QSO2237+0305, using the* `microlens` *code (Wambsganss, 1999).*

QSO2237+0305, aka the Einstein cross, is a priviledged target for microlensing studies because of the short time delays between its lensed images (e.g., Vakulik et al., 2006), and is known to exhibit microlensing variations (e.g., Irwin et al. 1989). Moreover, differential microlensing was detected through the velocity structure of the high-ionization carbon lines (Sluse et al. 2011, O'Dowd et al. 2011).

Method

We combine optical and near-IR spectra of the four images of QSO2237+0305 obtained in 2009 (Fig. 2) to compare microlensing measurements in emission lines with different ionization degrees.
The largest microlensing effect is detected in image A. Image D is supposed unaffected by microlensing and used as the reference.
We use the macro-micro decomposition method (MmD) described in Hutsemékers et al. (2010) to derive the part of the quasar spectrum that is microlensed in image A relatively to image D.

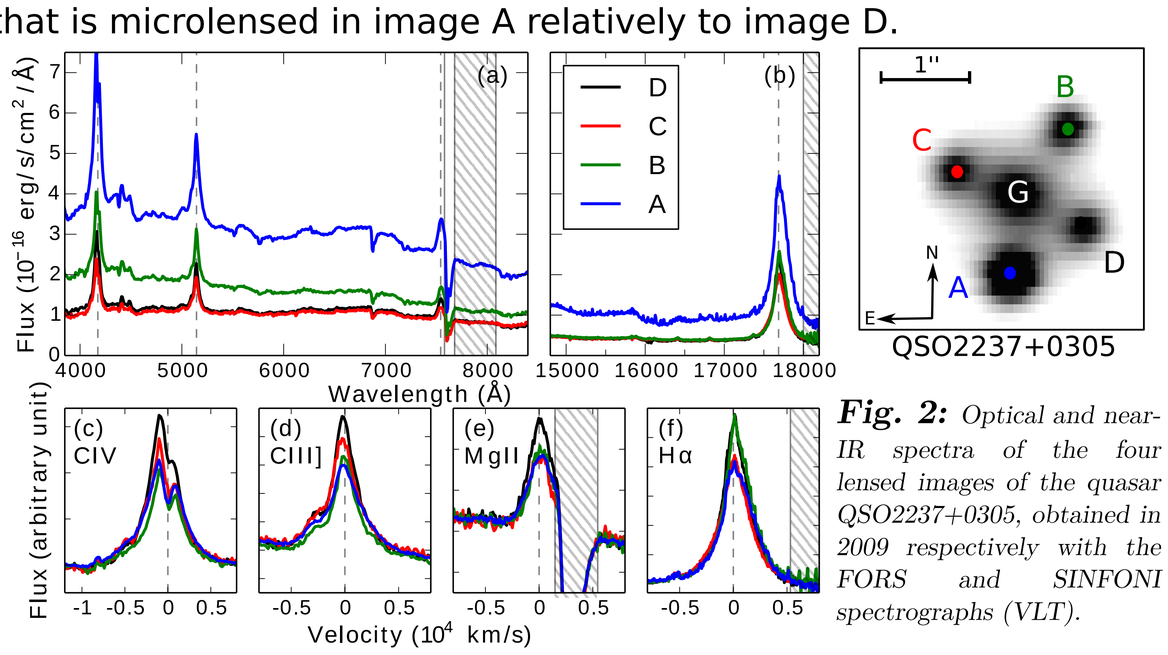

Fig. 2: *Optical and near-IR spectra of the four lensed images of the quasar QSO2237+0305, obtained in 2009 respectively with the FORS and SINFONI spectrographs (VLT).*

The macro-micro decomposition method

MmD assumes that the spectrum of each quasar image is a linear combination of a spectral component, F_M, that is only macrolensed, and a spectral component, $F_{M\mu}$, that is both macrolensed and microlensed:

$$F_A = M\,F_M + M\mu\,F_{M\mu} \quad (1)$$
$$F_D = F_M + F_{M\mu} \quad (2)$$

M is the macro-amplification ratio and μ the additional magnification due to microlensing. F_M and $F_{M\mu}$ can then be deduced from the spectra of images A and D, by inverting equations (1) and (2).
Fixing M=1, as suggested by macro-models and mid-infrared measurements (Agol et al. 2000), and supposing that the continuum is microlensed, a reasonable hypothesis considering that the continuum source is more compact than the BLR and thus more prone to microlensing (e.g. Kaspi et al. 2000, Sluse et al. 2011), μ is determined as the flux ratio computed in the continuum adjacent to the emission line.

Results

Wing/Core effect in CIV

F_M holds part of the CIV line core emission, which indicates that the line core is microlensed to a lesser degree than the wings, entirely included in $F_{M\mu}$. The comparable magnification of the continuum and of the highly blueshifted and red-shifted line flux requires their emission regions to be co-spatial or located close to each other, so that they sample same area of the caustic pattern.

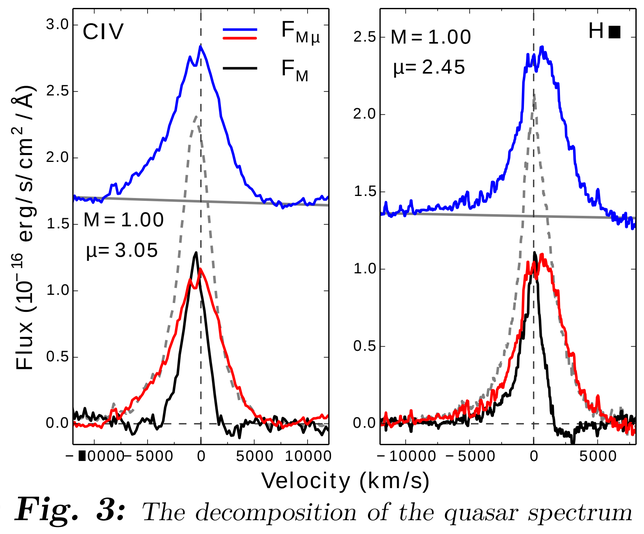

Fig. 3: *The decomposition of the quasar spectrum into a spectral component that is both macrolensed and microlensed in image A, $F_{M\mu}$ (blue), and a spectral component that is only macrolensed, F_M (black). The microlensed part of the broad line profile is emphasized by subtracting the continuum emission from $F_{M\mu}$ (red line).*

Red/Blue effect in Hα

The highly redshifted part of the Hα line, included in FMμ, is magnified as the continuum whereas the line core and blue wing are partly contained in both F_M and $F_{M\mu}$ and thus less microlensed.
The differential magnification of the highly blueshifted and red-shifted parts of the Hα line requires the approaching and receding parts of the velocity field of the low-ionization region to be spatially separated in projection. In addition, the emission region of the highly redshifted line flux should be located close to the continuum source so that the red wing and continuum undergo similar magnification.

Given that the same microlensing pattern magnifies both the high- and low-ionization regions, the dissimilar microlensing effects observed in CIV and Hα suggest that they have different geometries and/or kinematics. (For details see Braibant et al., 2016)

Table 1: *Comparing the constraints set by microlensing on the high- and low-ionization region to BLR models.*

The low-ionization region			
BLR models / **Contraints set by microlensing**	Keplerian disk	Polar Wind	Equatorial Wind
approaching and receding parts of the velocity field are spatially separated	✓	✗	✓
emission region of the highly redshifted part of the line close to the continuum source (in projection)	✓	If specific inclination (line of sight grazing the outflow biconical shell)	✗
The high-ionization region			
BLR models / **Contraints set by microlensing**	Keplerian disk	Polar Wind	Equatorial Wind
Fastly approaching and receding parts of the velocity field are co-spatial or close to each other (in projection)	✓	✓	✗
high velocities, negative and positive, are co-spatial with the continuum source or close to it (in projection)	✓	✓	✗
geometry/kinematics differs from that of the low-ionization region	✗	✓	✓

The constraints set by the symmetric micro-lensing effect observed in CIV and by the asymmetrical microlensing magnification of the Hα line favor a Keplerian disk for the low-ionization region and a polar wind for the high-ionization region (Table 1).
This is supported by simulations. The emission of a Keplerian disk, an equatorial wind and polar wind is simulated in several velocity slices using the `STOKES` code (Marin et al, 2012, Goosmann et al. 2013). When convolved by a caustic network, the number of synthetic distorted line profiles that match the distortions observed in Hα clearly favors the Keplerian disk model. (Braibant et al., in prep.)

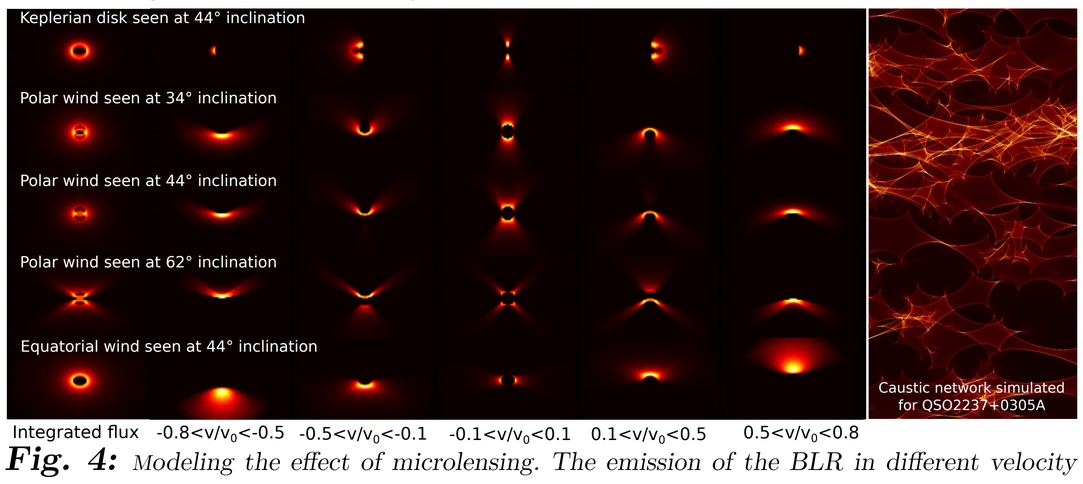

Fig. 4: *Modeling the effect of microlensing. The emission of the BLR in different velocity slices sampling the broad line is simulated using the* `STOKES` *radiative transfer code, and convolved by a synthetic caustic network.*